Loading of large ion Coulomb crystals into a linear Paul trap incorporating an optical cavity

ARTICLE *in* APPLIED PHYSICS B · NOVEMBER 2008

Impact Factor: 1.86 · DOI: 10.1007/s00340-008-3199-8 · Source: arXiv

Appl Phys B (2008) 93: 373–379
DOI 10.1007/s00340-008-3199-8

Applied Physics B
Lasers and Optics

Loading of large ion Coulomb crystals into a linear Paul trap incorporating an optical cavity

P. Herskind · A. Dantan · M.B. Langkilde-Lauesen · A. Mortensen · J.L. Sørensen · M. Drewsen

Received: 31 January 2008 / Revised version: 10 June 2008 / Published online: 13 September 2008

Abstract We report on the loading of large ion Coulomb crystals into a linear Paul trap incorporating a high-finesse optical cavity ($\mathcal{F} \sim 3000$). We show that, even though the 3-mm diameter dielectric cavity mirrors are placed between the trap electrodes and separated by only 12 mm, it is possible to produce in situ ion Coulomb crystals containing more than 10^5 calcium ions of various isotopes and with lengths of up to several millimeters along the cavity axis. We show that the number of ions inside the cavity mode is, in principle, high enough to achieve strong collective coupling between the ion Coulomb crystal and the cavity field. The results thus represent an important step towards ion trap based Cavity Quantum ElectroDynamics (CQED) experiments using cold ion Coulomb crystals.

PACS 32.80.Fb · 37.10.Ty · 42.50.Pq

1 Introduction

In recent years there has been much focus on light–matter interactions at the level of single photons, primarily motivated by applications within quantum information science, where an efficient light–matter interface is indispensable for many applications [1, 2]. Of particular interest has been the so-called strong coupling regime of Cavity Quantum ElectroDynamics (CQED) [3], in which the rate of coherent evolution within the system exceeds that of any dissipative processes, making this regime ideal for the quantum engineering of light–matter interfaces. A strong collective coupling between a medium of N atoms and the light field can be achieved if the single atom–photon coupling strength g_0 is large enough to satisfy the inequality $g_0\sqrt{N} > \gamma, \kappa$, where γ and κ are the decay rates of the atomic dipole and the cavity field, respectively. For optical frequencies, experiments with neutral atoms have been extremely successful and have reached the strong coupling regime for single atoms [4]. Such experiments benefit from the use of cavities of extremely small mode volumes to increase the single atom–photon coupling strength, given by: $g_0 = \frac{D}{\hbar}\sqrt{\frac{\hbar\omega}{2\epsilon_0 V}}$, where D is the transition dipole moment, ω is the frequency of the transition, and V is the mode volume of the cavity. However, since the cavity decay rate is inversely proportional to the cavity length, such experiments require very high finesse cavities, which are technically challenging to operate. One further complication of such experiments is the difficulty in efficiently trapping and confining the neutral atoms inside the cavity. While short-time solutions to this problem have recently been found [5, 6], ions, by contrast, can be stored for hours in ion traps and offer relatively easy access to a regime in which the spatial extent of their wave packet is well-localized on the scale of the optical wavelength of their atomic transition (Lamb–Dicke regime). Though experiments with single ions in cavities have confirmed this [7, 8], the strong coupling regime has not yet been reached, mainly due to the difficulty in lowering the mode volume, i.e., minimizing the mirror separation, without severely modifying the trapping potential, which makes trapping extremely challenging. The requirement of a small mode volume can be relaxed for ensembles of atoms or ions due to the $\sqrt{N}$ factor entering in the collective coupling strength of the ensemble. This means that a technically less demanding longer cavity with a lower finesse can be used in

P. Herskind (✉) · A. Dantan · M.B. Langkilde-Lauesen · A. Mortensen · J.L. Sørensen · M. Drewsen
QUANTOP, Danish National Research Foundation Center for Quantum Optics, Department of Physics and Astronomy, University of Aarhus, 8000 Århus C., Denmark
e-mail: herskind@phys.au.dk

such experiments.

In addition to the issue of tight confinement and long storage time, ion Coulomb crystals have a number of advantages over cold atomic samples. As the ions are confined in a crystal lattice, the decoherence rate due to collisions is very low. Furthermore, the lattice structure in conjunction with the standing wave field of the optical resonator might be interesting for the engineering of the atom–photon interaction. Whereas spatial structuring would require the use of optical lattices for neutral atoms, it is inherent in an ion Coulomb crystal and as described in a recent paper [9], the structure of ion Coulomb crystals can be made very regular and periodic. Finally, the low optical density of the ion Coulomb crystal ($\sim 10^8$ cm^{-3}) makes optical pumping and state preparation unproblematic.

In this paper we focus on the production and characterization of large cold ensembles of ions, specifically ion Coulomb crystals, of up to hundreds of thousands of ions in a linear Paul trap incorporating a high finesse optical cavity designed for CQED experiments. We show that it is possible to insert cavity mirrors in-between the trap electrodes without significantly perturbing the trapping fields, that the ion Coulomb crystals can be produced in a clean and efficient way that preserves the finesse of the cavity, and that the number of ions in the cavity mode can be high enough to potentially satisfy the strong coupling criterion $g_0\sqrt{N} > \gamma, \kappa$. These results thus represent an important step towards ensemble-based CQED with ion Coulomb crystals and open up for the use of such media as a tool for quantum information processing [10–12].

The paper is organized as follows: In Sect. 2, we describe our linear Paul trap along with the integrated cavity. In Sect. 3, we describe the loading scheme used for the production of the Coulomb crystals of calcium ions and present results on loading of the trap with various naturally abundant calcium isotopes. In Sect. 4, we address the issue of optimization of the loading in terms of maximizing the total number of ions within the cavity mode volume. In Sect. 5, we conclude.

2 Experimental setup

Figure 1 shows a sketch of the setup used in the experiments. The trap is a linear Paul trap [13] which consists of 4 sectioned cylindrical electrode rods placed in a quadrupole configuration. The length of the center-electrode is $z_0 = 5.0$ mm, and the length of the end-electrodes is $z_E = 5.9$ mm. The electrode diameter is $d = 5.2$ mm and the distance from the trap center to the electrodes is $r_0 = 2.35$ mm. Confinement in the radial plane (xy-plane in Fig. 1) is obtained by applying time varying voltages $\frac{1}{2}U_{\rm rf}\cos(\Omega_{\rm rf}t)$ and $\frac{1}{2}U_{\rm rf}\cos(\Omega_{\rm rf}t + \pi)$ to the two sets of diagonally opposite

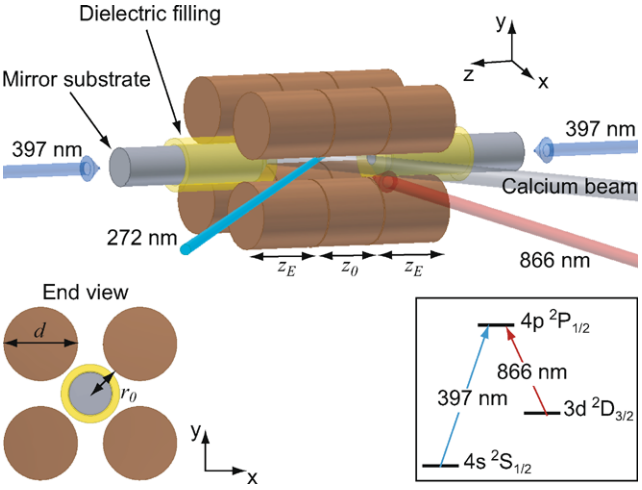

Fig. 1 Schematic of the linear Paul trap with laser and atomic beams indicated. The dielectric fillings have been included to minimize the rf-fields along the trap axis (z-axis). The *insert* shows the level scheme used in Doppler laser cooling of Ca^+

electrode rods. The sectioning of each of the electrode rods allows for application of a static voltage $U_{\rm end}$ to the end-electrodes, which provides confinement along the z-axis. The potential along the z-axis is well described by

$$\Phi_z(z) = \frac{1}{2}M\omega_z^2 z^2, \qquad \omega_z^2 = \frac{2\eta Q U_{\rm end}}{M z_0^2}, \tag{1}$$

where M and Q are the mass and charge of the ion and $\eta = 0.342$ is a constant related to the trap geometry. For $2QU_{\rm rf}/Mr_0^2\Omega_{\rm rf}^2 \ll 1$ one can introduce an effective or pseudo-potential in the radial plane described by [14]

$$\Phi_r(r) = \frac{1}{2}M\omega_r^2 r^2, \qquad \omega_r^2 = \frac{Q^2U_{\rm rf}^2}{2M^2r_0^4\Omega_{\rm rf}^2} - \frac{\eta Q U_{\rm end}}{M z_0^2}. \tag{2}$$

In such a three-dimensional potential, one finds that the density of ions in an ion Coulomb crystal is controlled only by the rf-voltage and given by[15]

$$\rho = \frac{\epsilon_0 U_{\rm rf}^2}{M r_0^4 \Omega_{\rm rf}^2}. \tag{3}$$

The trap is operated at a frequency $\Omega_{\rm rf} = 2\pi \times 4.0$ MHz and the end-voltage $U_{\rm end}$ is typically 1 to 10 V. The rf-voltage $U_{\rm rf}$ is typically between 100 and 400 V, which leads to ion densities between 6.9×10^7 and 1.1×10^9 cm^{-3}.

The unique feature of this trap is the incorporation of a high finesse optical cavity, with mirrors situated in between the electrodes. The cavity is designed for operating on the 3d $^2D_{3/2} \rightarrow$ 4p $^2P_{1/2}$ transition of $^{40}Ca^+$ at 866 nm (see insert of Fig. 1). The mirrors, both with a radius of curvature of 10 mm, are placed in a near-confocal geometry supporting a standing wave mode of light at 866 nm with a waist of $\sim$37 μm at the trap center. The transmission of the two

mirrors is 1500 ppm and 5 ppm at 866 nm, respectively. One mirror can be translated axially by applying a voltage to a set of piezoelectric transducers (PZT) holding the mirror mount. Figure 2 shows a cavity scan across one free spectral range (FSR). The mode matching of the cavity to the fundamental TEM_{00} mode is $\simeq$98% compared to higher order modes. The cavity finesse at 866 nm is determined by measuring the FSR and the width of the resonance peak. The FSR is measured to be $\Delta\nu_{FSR} = (12.7 \pm 0.3)$ GHz, corresponding to a cavity length of 11.8 mm. This value was obtained by tuning the laser frequency over one FSR of the cavity while recording the number of (known) FSR of a longer reference cavity. The insert in Fig. 2 shows a scan around the cavity resonance while the laser is modulated at 5 MHz. The resulting sidebands provide a frequency calibration and from a multipole Lorentzian fit we deduce a cavity width of $\delta\nu = (4.2 \pm 0.2)$ MHz. The resulting finesse is then $\mathcal{F} = \Delta\nu_{FSR}/\delta\nu = 3000 \pm 200$. This is also consistent with the incoupling mirror transmission of 1500 ppm and intra-cavity losses of 600 ppm, which we derived from the cavity reflection signal. The intra-cavity losses are due to mirror contamination introduced mainly during degassing of the ion pump connected to the vacuum chamber and will be avoided in the future by inserting a valve between the ion pump and the trap chamber. Since this initial contamination, intra-cavity losses have been observed to increase slowly. In terms of experimental hours where the oven has been turned on, the rate is estimated to be $\sim$0.1 ppm/hour. Whether this contamination originates from atomic calcium from the oven, from calcium ions lost from the trap, or from the background pressure ($\sim 5 \times 10^{-10}$ mbar) is at present not known. Based on the measurements quoted above, we deduce a cavity decay rate of $\kappa = 2\pi \times (2.1 \pm 0.1)$ MHz. From the spontaneous decay rate Γ of the excited 4p $^2P_{1/2}$ state of $^{40}Ca^+$, the decay rate for the atomic dipole is $\gamma = \Gamma/2 = 2\pi \times 11$ MHz. From the dimensions of the cavity, the ion–photon coupling strength of a single $^{40}Ca^+$ ion at the cavity waist and field anti-node is expected to be $g_0 = 2\pi \times 0.53$ MHz. In principle, it thus requires $N \simeq 500$ ions within the cavity mode volume to enter a regime governed by a strong collective coupling (where $g_0\sqrt{N} > \gamma, \kappa$ is satisfied).

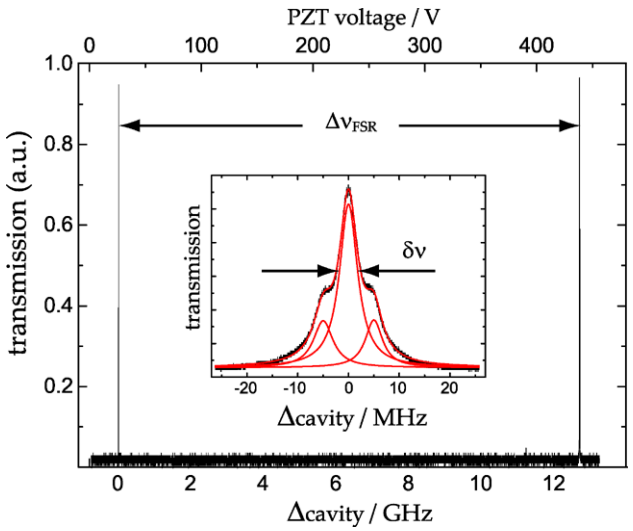

Fig. 2 Scan across a FSR of the cavity. The *insert* shows a scan around the cavity resonance while the laser was modulated at 5 MHz. The FSR is measured to be $\Delta\nu_{FSR} = (12.7 \pm 0.3)$ GHz and the cavity width is $\delta\nu = (4.2 \pm 0.2)$ MHz

3 Loading of the trap

In order to efficiently load large crystals into the trap we employ the technique of resonance-enhanced photoionization [16]. As compared to conventional electron bombardment, this method has several advantages which are all essential to the experiment. First of all, the problem of charging surrounding isolating materials, e.g., mirror substrates, is greatly reduced as only a single electron is produced per ion [16, 17]. Secondly, the ionization efficiency can be made much higher, leading to loading rates which are significantly higher than what can be achieved with electron bombardment [18]. This makes loading at a lower atomic flux practical [19] and thus reduces the risk of contaminating both the trap electrodes and closely spaced delicate objects, such as the mirrors integrated into the ion trap. While deposition of material on the electrodes is suspected to give rise to heating of the ions [20, 21], contamination of the mirrors will lower the quality of the resonator. Finally, the technique can be extremely isotope selective [22], allowing for loading of different isotopes in well-controlled ratios.

The level scheme used in this work for photoionization is presented in Fig. 3. A single UV-light source at 272 nm ionizes atomic calcium in a two-photon process through resonant excitation of the 4s5p $^1P_1$ state followed by absorption of a second 272 nm photon from either the 4s5p $^1P_1$ state or the 4s3d $^1D_2$ state (populated through spontaneous

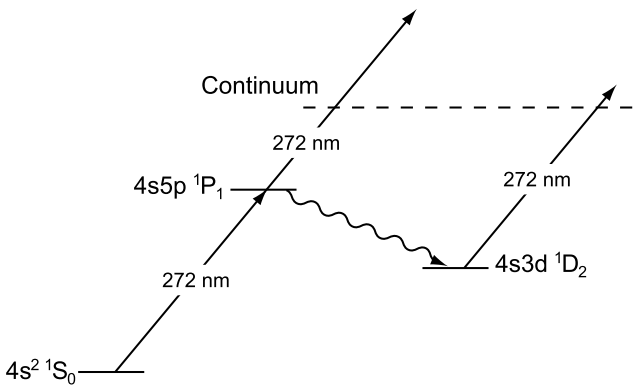

Fig. 3 Resonant two-photon ionization scheme used in this work

emission) into the continuum (see Fig. 3) [16, 22]. The light at 272 nm originates from a laser system based on a commercial Ytterbium-doped DFB fiber laser that has been frequency doubled twice to produce light at the fourth harmonic. The DFB fiber laser system was described in detail in a recent paper [23]. In brief, light from a CW DFB fiber laser operating at 1088 nm is first frequency doubled in a bow-tie cavity containing a $LiNbO_3$ crystal to produce light at 544 nm. This light is subsequently frequency doubled in a bow-tie cavity containing a β-$BaBa_2O_4$ crystal to finally produce light at 272 nm. Frequency tuning can be achieved by controlling the length of the fiber laser cavity either with a PZT, or by changing the temperature.

For loading of the trap, a thermal beam of atomic calcium with a cross section of $\sim 1.0 \times 1.5$ mm^2 is intersected by the 272 nm laser beam in the center of the trap at right angles in order to minimize Doppler broadening. The atomic beam is produced from an effusive oven followed by a series of skimmers, inserted to avoid deposition of calcium on the trap electrodes and cavity mirrors. The UV-beam has a power of about 20 mW and a waist of $\sim$160 μm at the trap center. The ions produced are then Doppler laser cooled on the 4s $^2S_{1/2} \rightarrow$ 4p $^2P_{1/2}$ transition along the trap axis (z-axis in Fig. 1) by two counter propagating beams at 397 nm (beam diameter $\sim$1 mm), while in the radial plane (xy-plane in Fig. 1) the ions are sympathetically cooled through the Coulomb interaction. An 866 nm beam, resonant with the 3d $^2D_{3/2} \rightarrow$ 4p $^2P_{1/2}$ transition, is applied to prevent the ions from being shelved into the metastable $D_{3/2}$ state (see insert of Fig. 1). Typically, 8–10 mW of 397 nm light detuned by $\sim$20−40 MHz below resonance is used during loading. Both power and detuning are then decreased upon completion of the loading in order to optimize the cooling. Detection of the ions is performed by imaging spontaneously emitted light at 397 nm onto an image intensified CCD camera located above the trap in Fig. 1. The number of ions loaded can then be deduced from the recorded images by the method described in [24].

Figure 4 shows the number of loaded ions versus time when the frequency of the 272 nm light source is tuned close to the resonance of the 4s^2 $^1S_0 \rightarrow$ 4s5p $^1P_1$ transition of ^{40}Ca. The end- and rf-voltages were $U_{\mathrm{end}} = 3.9$ V and $U_{\mathrm{rf}} = 130$ V, respectively ($\omega_r = 2\pi \times 225$ kHz and $\omega_z = 2\pi \times 160$ kHz), and the oven temperature during the loading sequence was 400°C. As can be seen from the figure, we are able to load in the excess of 3000 ions/s at this relatively low oven temperature. This means that Coulomb crystals with more than 10^5 ions can be produced within a minute. Figure 5 shows an example of such a crystal, where the total number of ions is 88000 and the density and length of the crystal are 6.2×10^8 cm^{-3} and 3 mm, respectively.

A potentially attractive feature of ion Coulomb crystal based CQED is the possibility to work with crystals of various isotope contents. Two-component crystals are especially

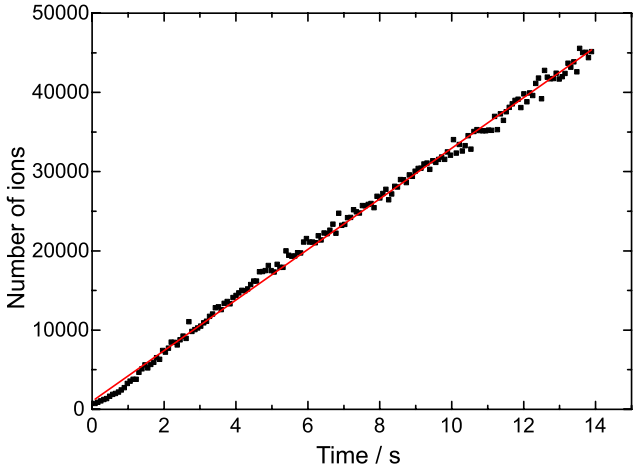

Fig. 4 Number of ions loaded versus time when the ionization laser frequency is tuned close to the 4s^2 $^1S_0 \rightarrow$ 4s5p $^1P_1$ transition of ^{40}Ca. The UV-power used for ionization was 20 mW and the oven temperature 400°C. The loading rate deduced from the linear fit is $\sim$3200 ions/s

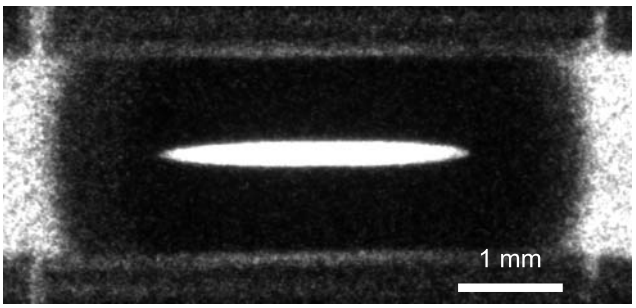

Fig. 5 Image of a 3 mm long $^{40}Ca^+$ Coulomb crystal with 88000 ions. The rf- and end-voltages are 300 V and 1.7 V, respectively. The visible features outside the crystal region are from the trap and due to light scattered from the 397 nm beams as they pass through the mirrors. Due to the low magnification needed to image the whole crystal, no detailed crystal structure is visible

interesting for CQED studies since they allow for laser cooling one component (outer, radially separated component) while having the other component (inner cylindrical component) interacting with the cavity field only. By tuning our 272 nm light source to resonance with the respective transitions of specific isotopes of calcium, we have loaded such two-component crystals consisting of $^{40}Ca^+$ and isotopes of higher mass numbers. When producing $^M Ca^+$, where $M > 40$, $^{40}Ca^+$ ions are also created through an electron charge transfer process between atoms in the atomic beam, dominated by ^{40}Ca, and the ions in the trap [22]. This process has the form, $^{40}Ca + {}^M Ca^+ \rightarrow {}^{40}Ca^+ + {}^M Ca + \Delta E^M$ and is nearly resonant in the sense that ΔE^M lies much below the energy associated with the thermal collisions leading to the exchange process. The relative content of $^{40}Ca^+$ and less naturally abundant isotopes in the crystal can be controlled to a high degree by turning on the atomic beam

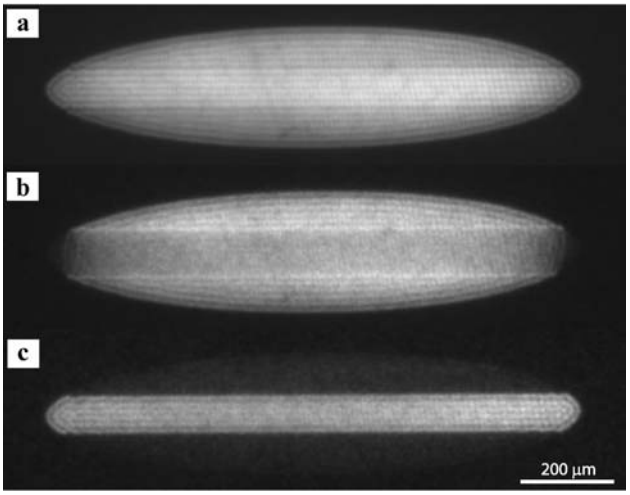

Fig. 6 (**a**) Image of a two-component crystal consisting of ∼2000 $^{40}Ca^{+}$ (inner component) and ∼13000 $^{44}Ca^{+}$ (outer component) that are being laser cooled simultaneously (16 s exposure time). (**b**) $^{44}Ca^{+}$ laser cooled, $^{40}Ca^{+}$ sympathetically cooled (1 s exposure time). (**c**) $^{40}Ca^{+}$ laser cooled, $^{44}Ca^{+}$ sympathetically cooled (1 s exposure time). For technical reasons the cooling light resonant with the sympathetically cooled component was not turned off completely and in both (**b**) and (**c**) this component is still weakly visible

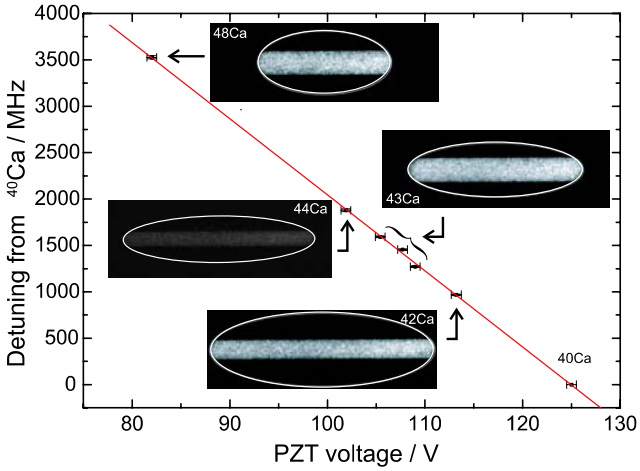

Fig. 7 Frequency detuning with respect to the ^{40}Ca resonance vs. voltage applied to the fiber laser PZT. The three points around ^{43}Ca correspond to the different hyperfine splitting of the 4s5p $^{1}P_1$ level and the frequency shifts of the various isotopes with respect to the ^{40}Ca resonance are taken from [22]. The fit indicates a frequency shift of 82 ± 2 MHz/V at 272 nm and the error bars reflect the uncertainty in determining the peak of the ionization resonance. Inserts show typical two-component crystals of the various isotopes, for the same rf-voltage of 220 V, but unequal end-voltages. The dimensions of the black frames are 1.4 mm × 0.5 mm and the ellipsoids indicate the boundaries of the outer component of the two-component crystals

after the ionization laser has been turned off. Due to the mass dependence of the radial trapping potential (cf. (2)) the different isotopes separate radially when cooled into an ion Coulomb crystal [15]. This is clearly seen in Fig. 6(a) where both $^{40}Ca^{+}$ and $^{44}Ca^{+}$ ions are laser cooled simultaneously. In Fig. 6(b) and 6(c) the cooling lasers have been applied only to one component, while the other is being sympathetically cooled. Two-component crystals of $^{40}Ca^{+}$ ions and all other naturally abundant isotopes of calcium (except $^{46}Ca^{+}$ which has a natural abundance of only $\sim 10^{-5}$ [25]) have been produced through the charge transfer process described above, as seen in Fig. 7. The laser system is capable of covering the entire spectrum of naturally abundant calcium and allows for easy and quick changing from one isotope to another, which makes CQED studies with such two-components crystals practical. The relevant transition for the CQED experiments on this system is the 3d $^{2}D_{3/2} \rightarrow$ 4p $^{2}P_{1/2}$ transition of Ca^{+}. The isotope shift of this transition, relative to $^{40}Ca^{+}$, is 4.5 GHz for $^{44}Ca^{+}$, which means that $^{40}Ca^{+}$ should not be affected by the cooling lasers when this component is being sympathetically cooled by the $^{44}Ca^{+}$ ions. However, with our loading scheme we have the possibility to work with $^{48}Ca^{+}$ instead of $^{44}Ca^{+}$ which has an even larger isotope shift of 8.3 GHz [26].

As mentioned previously, compared to electron bombardment, the method of resonant photoionization minimizes charging effects as well as trap contamination and formation of patch potentials. From the images shown in Figs. 6 and 7, there appears to be no visible perturbation on the shape caused by such effects. In Fig. 6 the upper and lower boundaries of the inner component have been measured to be parallel at least to within 2 mrad, indicating that the introduction of cavity mirrors inside a linear Paul trap does not significantly perturb the trapping of such crystals.

4 Optimizing the total number of ions inside the cavity mode

As mentioned in the introduction, one of the main challenges for the realization of CQED with ion Coulomb crystals is to load a large number of ions into the cavity mode to enhance the collective atom–light coupling. For our trap, with the optical cavity axis coinciding with the trap axis, the highest number of ions in the cavity mode is achieved when the product of the crystal length and the density ρ is maximized. The length is controlled by both the end- and rf-voltage, whereas the density is determined solely by the rf-voltage (cf. (3)). Ideally, we would therefore wish to work at a very low U_{end} and a very high U_{rf}. In practice, we find that the crystals become unstable at lengths above a few mm, although the exact length is very dependent on the rf-voltage and on the total number of ions in the crystal as well as the level of cooling power. In qualitative terms, we interpret this as a result of rf-heating in the crystal [27, 28]. This heating drives the radial motion of the ions, while the laser cooling beams act only directly along the trap axis (see Fig. 1). Since the coupling between axial and radial motion is weaker for longer than for shorter prolate crystals,

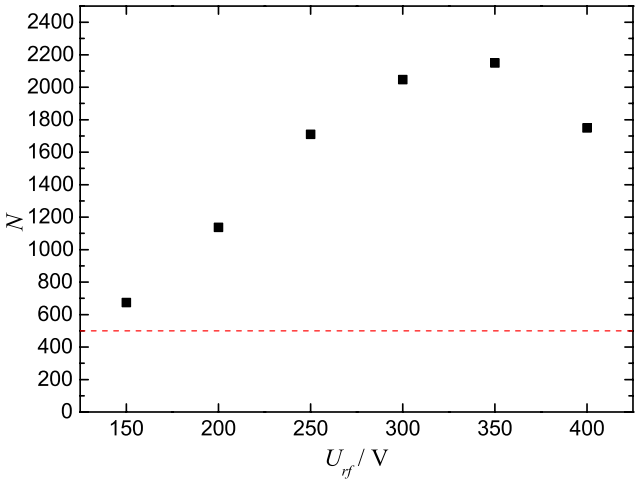

Fig. 8 Number of ions N in the cavity mode volume versus rf-voltage $U_{\rm rf}$. The interval from 150 to 400 V corresponds to ion densities between $1.6 \times 10^8 - 1.1 \times 10^9$ cm^{-3}. The *dashed line* indicate the level above which the criterium for strong collective coupling is potentially satisfied

compensation of rf-heating by axial laser cooling is less efficient in longer prolate crystals. Increasing the cooling power may help to confine longer crystals containing more ions, however, there is ultimately a tradeoff between the maximal attainable length, the total number of crystalized ions, and the ion density. Figure 8 shows the maximal attainable number of ions in the cavity mode[1] N as a function of rf-voltage $U_{\rm rf}$ (density ρ). Each point was found by lowering the end-voltage and letting the crystal expand axially until it became unstable and was lost. The number of ions in the cavity mode is found to be maximal for rf-voltages around 350 V ($\rho \simeq 8.5 \times 10^8$ cm^{-3}). Here, more than 2000 ions are in the cavity mode, which would correspond to a collective coupling strength of $g_0\sqrt{N} \simeq 2\pi \times 24$ MHz. The dashed line in the figure indicates the level above which the number of ions becomes large enough to satisfy the strong collective coupling criterium.

5 Conclusions

We have achieved efficient in situ loading of large ion Coulomb crystals in a linear Paul trap with an integrated optical resonator. This work demonstrates that such a high finesse optical cavity can be incorporated into a linear Paul trap without impeding the trapping of large ion Coulomb crystals and that these crystals can have lengths comparable to that of the cavity (more than one third of the cavity length). A small increase in the intra-cavity losses has been observed over several months, though the origin of this contamination is still unclear. However, the low level of contamination observed does not represent a significant obstacle for fulfilling the criteria for strong collective coupling within the system as the resulting decay rate of the cavity is still sufficiently low. Finally, we have investigated the optimal trapping parameters for maximizing the number of ions in the cavity mode and found that more than 2000 ions could be confined within the cavity mode volume. This number indicates that the system should be able to enter the strong collective coupling regime and opens up for the possibility of CQED experiments with ion Coulomb crystals.

Acknowledgements The Authors would like to thank Joan Marler and Magnus Albert for useful discussions and for proofreading the manuscript.

This work has been financially supported by The Carlsberg Foundation.

References

1. J.I. Cirac, P. Zoller, H.J. Kimble, H. Mabuchi, Phys. Rev. Lett. **78**, 3221 (1997)
2. L.-M. Duan, M.D. Lukin, J.I. Cirac, P. Zoller, Nature **414**, 413 (2001)
3. P.R. Berman (ed.), *Cavity Quantum Electrodynamics* (Academic, London, 1994)
4. H.J. Kimble, Phys. Scr. T **76**, 127 (1998)
5. A.D. Boozer, A. Boca, R. Miller, T.E. Northup, H.J. Kimble, Phys. Rev. Lett. **97**, 083602 (2006)
6. T. Puppe, I. Schuster, A. Grothe, A. Kubanek, K. Murr, P.W.H. Pinkse, G. Rempe, Phys. Rev. Lett. **99**, 013002 (2007)
7. M. Keller, B. Lange, K. Hayasaka, W. Lange, H. Walther, Appl. Phys. B **76**, 125 (2003)
8. A.B. Mundt, A. Kreuter, C. Russo, C. Becher, D. Leibfried, J. Eschner, F. Schmidt-Kaler, R. Blatt, Appl. Phys. B **76**, 117 (2003)
9. A. Mortensen, E. Nielsen, T. Matthey, M. Drewsen, J. Phys. B: At. Mol. Opt. Phys. **40**, F223 (2007)
10. A. Mortensen, *Aspects of ion Coulomb crystal based quantum memory for light*. PhD thesis, Department of Physics and Astronomy, University of Aarhus (2005)
11. P. Herskind, A. Mortensen, J.L. Sørensen, M. Drewsen, Cavity-QED with ion Coulomb crystals, in *Non-Neutral Plasma Physics Conference IV*, AIP Conference Proceedings, vol. 862, p. 292 (2006)
12. T. Coudreau, F. Grosshans, S. Guibal, L. Guidoni, J. Phys. B: At. Mol. Opt. Phys. **40**, 413 (2007)
13. J.D. Prestage, G.J. Dick, L. Maleki, J. Appl. Phys. **66**, 1013 (1989)
14. M. Drewsen, A. Brøner, Phys. Rev. A **62**, 045401 (2000)
15. L. Hornekær, N. Kjærgaard, A.M. Thommesen, M. Drewsen, Phys. Rev. Lett. **86**, 1994 (2001)
16. N. Kjærgaard, L. Hornekær, A.M. Thommesen, Z. Videsen, M. Drewsen, Appl. Phys. B **71**, 207 (2000)
17. M. Brownnutt, V. Letchumanan, G. Wilpers, R.C. Thompson, P. Gill, A.G. Sinclair, Appl. Phys. B **87**, 411 (2007)
18. R.J. Hendricks, D.M. Grant, P.F. Herskind, A. Dantan, M. Drewsen, Appl. Phys. B **88**, 507 (2007)

[1] N is defined through the definition of the collective coupling strength $g_0\sqrt{N} = g_0\sqrt{\rho \int \Psi(\mathbf{r})^2 \, d\mathbf{r}}$, where the standing wave TEM$_{00}$ mode function is given by $\Psi = \frac{w_0}{w(z)} e^{-(x^2+y^2)/w(z)^2} \sin(kz)$ and where the integral is evaluated over the crystal length l. With this definition $N = \rho \frac{\pi w_0^2}{4} l$.

19. S. Gulde, D. Rotter, P. Barton, F. Schmidt-Kaler, R. Blatt, W. Hogervosrt, Appl. Phys. B **73**, 861 (2001)
20. L. Deslauriers, S. Olmschenk, D. Stick, W.K. Hensinger, J. Sterk, C. Monroe, Phys. Rev. Lett. **97**, 103007 (2006)
21. R.G. DeVoe, C. Kurtsiefer, Phys. Rev. A **65**, 063407 (2002)
22. A. Mortensen, J.J.T. Lindballe, I.S. Jensen, P. Staanum, D. Voigt, M. Drewsen, Phys. Rev. A **69**, 42502 (2004)
23. P. Herskind, J. Lindballe, C. Clausen, J.L. Sørensen, M. Drewsen, Opt. Lett. **32**, 268 (2007)
24. D.N. Madsen, S. Balslev, M. Drewsen, N. Kjærgaard, Z. Videsen, J.W. Thomsen, J. Phys. B: At. Mol. Opt. **33**, 4981 (2000)
25. J. Emsley, *The Elements Oxford Chemistry Guides* (Oxford University Press, New York, 1995)
26. W. Nörtershaüser, K. Blaum, K. Icker, P. Müller, A. Schmitt, K. Wendt, B. Wiche, Eur. Phys. J. D **2**, 33 (1998)
27. R. Blümel, C. Kappler, W. Quint, H. Walther, Phys. Rev. A **40**, 808 (1989)
28. J.P. Schiffer, M. Drewsen, J.S. Hangst, L. Hornekær, Proc. Natl. Acad. Sci. **97**, 10697 (2000)